Biophysical properties of $Ca_V1.3$ calcium channels in gerbil inner hair cells

Stuart L. Johnson and Walter Marcotti

Department of Biomedical Science, University of Sheffield, Sheffield S10 2TN, UK

The Ca^{2+} current (I_{Ca}) in prehearing and adult inner hair cells (IHCs), the primary sensory receptors of the mammalian cochlea, is mainly carried by L-type ($Ca_V1.3$) Ca^{2+} channels. I_{Ca} in immature and adult IHCs triggers the release of neurotransmitter onto auditory afferent fibres in response to spontaneous action potentials (APs) or graded receptor potentials, respectively. We have investigated whether the biophysical properties of I_{Ca} vary between low- and high-frequency IHCs during cochlear development and whether its inactivation influences cellular responses. I_{Ca} was recorded from gerbil IHCs maintained near physiological recording conditions. The size of I_{Ca} in adult IHCs was about a third of that in immature cells with no apparent difference along the cochlea at both stages. The activation kinetics of I_{Ca} were significantly faster in high-frequency IHCs, with that of adult cells being more rapid than immature cells. The degree of I_{Ca} inactivation was similar along the immature cochlea but larger in high- than low-frequency adult IHCs. This inactivation was greatly reduced with barium but not affected by changing the intracellular buffer (BAPTA instead of EGTA). Immature basal IHCs showed faster recovery of I_{Ca} from inactivation than apical cells allowing them to support a higher AP frequency. I_{Ca} in adult IHCs was more resistant to progressive inactivation following repeated voltage stimulation than that of immature cells. This suggests that adult IHCs are likely to be suited for sustaining rapid and repeated release of synaptic vesicles, which is essential for sound encoding.

(Received 18 September 2007; accepted after revision 11 December 2007; first published online 3 January 2008)
Corresponding author W. Marcotti: Department of Biomedical Science, University of Sheffield, Sheffield S10 2TN, UK. Email: w.marcotti@sheffield.ac.uk

Inner hair cells (IHCs), the primary sensory receptors of the mature mammalian cochlea, are responsible for relaying acoustic information transduced by mechano-sensitive channels to the central nervous system via afferent auditory nerve fibres. This is driven by Ca^{2+} entering IHCs through Ca^{2+} channels in response to depolarizing receptor potentials initiated by hair bundle deflection. In immature mammalian IHCs of most rodents ($\leq$ P12: Mikaelian & Ruben, 1965; Woolf & Ryan, 1984) afferent synaptic transmission is driven by spontaneous Ca^{2+}-dependent action potentials (Glowatzki & Fuchs, 2002; Marcotti *et al.* 2003*b*; Johnson *et al.* 2005), which are likely to influence both the refinement of downstream neural circuits and intrinsic IHC development (Johnson *et al.* 2007) in analogy with other developing systems (Zhang & Poo, 2001; Moody & Bosma, 2005). Since voltage-gated Ca^{2+} channels play such a crucial role in immature and adult IHCs, any tonotopic and/or developmental differences in their biophysical properties are likely to have a significant impact on function. It is now well established that the majority ($\sim$90%) of the Ca^{2+} current in hair cells of both mammals (Platzer *et al.* 2000; Knirsch *et al.* 2007) and non-mammals (turtle: Schnee & Ricci, 2003; chick: Fuchs *et al.* 1990; Spassova *et al.* 2001; frog: Rodriguez-Contreras & Yamoah, 2001) is carried by L-type Ca^{2+} channels containing the $Ca_V1.3$ subunit (Kollmar *et al.* 1997; Platzer *et al.* 2000). The nature of the remaining $\sim$10% of non-L-type Ca^{2+} channels is still debatable since N-, R- and T-types have been described in hair cells of various vertebrates (Martini *et al.* 2000; Rodriguez-Contreras & Yamoah, 2001).

In vertebrates, the cochlear sensory neuroepithelium is tonotopically organized such that the characteristic frequency of HCs (the frequency at which they respond best) gradually changes with their position along the organ. In the non-mammalian cochlea the characteristic frequency of HCs is intrinsically dictated by the interplay between the relative number and kinetic properties (Wu *et al.* 1995) of both Ca^{2+} and BK channels (Art & Fettiplace, 1987; Fuchs *et al.* 1988) as well as local Ca^{2+} buffering kinetics (Ricci *et al.* 2000), which vary as a function of position along the cochlea. This inherent electrical tuning in lower vertebrate hair cell is not found in IHCs of the adult mammalian cochlea where their characteristic

 DOI: 10.1113/jphysiol.2007.145219

frequency is thought to be determined by the active mechanical amplification of the cochlea partition via the outer hair cells (Dallos, 1992). Although numerous studies have investigated Ca^{2+} channels in IHCs of the mammalian cochlea (Platzer *et al.* 2000; Marcotti *et al.* 2003*b*; Johnson *et al.* 2005) there is still an absence of information regarding any change in their biophysical properties as a function of the frequency position along the cochlea. However, a recent study using immunogold staining has shown that tonotopic differences exist at least in the concentration of Ca^{2+} buffering proteins in mammalian cochlear hair cells (Hackney *et al.* 2005).

The aim of this paper was to investigate the kinetic properties and Ca^{2+}-dependent inactivation of I_{Ca} in low- and high-frequency IHCs of the gerbil cochlea during development. This information would provide the first electrophysiological evidence for a position-dependent specialization intrinsic to the IHCs, the function of which could be to fine-tune the responses of these auditory receptors. All I_{Ca} recordings, apart from those designed to investigate its temperature dependence, were performed in near physiological conditions (body temperature and using 1.3 mM extracellular Ca^{2+}) to ensure a more realistic estimation of the channels biophysical properties.

Methods

Tissue preparation

Apical-coil and basal-coil inner hair cells (IHCs, $n = 133$) were studied in acutely dissected organs of Corti from Mongolian gerbils during development (from postnatal day 3 (P3) to P69, where the day of birth is P0). The reason for choosing the gerbil, instead of the more commonly used mouse, was due to their extended low-frequency hearing range that would emphasize any tonotopic differences (gerbil: ∼0.1–50 kHz; mouse: ∼2–100 kHz, Greenwood, 1990).

Gerbils were killed by cervical dislocation in accordance with UK Home Office regulations. The cochleae were dissected in normal extracellular solution (mM): 135 NaCl, 5.8 KCl, 1.3 $CaCl_2$, 0.9 $MgCl_2$, 0.7 NaH_2PO_4, 5.6 D-glucose, 10 Hepes-NaOH. Sodium pyruvate (2 mM), amino acids and vitamins (Eagle's MEM) were also added from concentrates (Fisher Scientific, Loughborough, UK). The pH was adjusted to 7.5 (osmolality ∼308 mosmol kg^{-1}). The dissected cochleae were transferred to a microscope chamber, immobilized under a nylon mesh attached to a stainless steel ring, and continuously perfused with a peristaltic pump using the above extracellular solution. The organs of Corti were viewed using an upright microscope (Leica DMLFS, Germany) with Nomarski optics (×63 objective). *In situ* recordings were made by exposing the basolateral surfaces of IHCs using a suction pipette (tip diameter about 4 μm), which was filled with extracellular solution. The approximate position of IHCs along the cochlea was recorded as fractional distance from the extreme base. Adult IHCs were positioned at a fractional distance of between 0.9 and 0.95 (apex) and between 0.1 and 0.2 (base), corresponding to a frequency range of 250 Hz and 420 Hz in apical and 20 kHz and 37 kHz in basal cells (Müller, 1996). Immature IHCs were recorded from a similar fractional distance to that of adult cells.

Electrical recording

Patch clamp recordings were performed near body temperature (34–37°C) using an Optopatch (Cairn Research Ltd, Faversham, UK) and an Axopatch 200B (Molecular Devices, USA) amplifier. A few experiments were conducted at room temperature (21–23°C) in order to determine the effect of temperature on the size of the Ca^{2+} current. The temperature dependence of I_{Ca} was described by its temperature coefficient (Q_{10}), which was calculated from the van't Hoff equation:

$$Q_{10} = (k_2/k_1)^{(10/(T_2-T_1))},$$

where k_1 and k_2 are the values I_{Ca} measured at the lower (T_1) and higher (T_2) temperatures, respectively.

Patch pipettes were made from soda glass capillaries (Harvard Apparatus Ltd, Edenbridge, UK) and had a typical resistance in extracellular solution of 2–3 MΩ. In order to reduce the electrode capacitance, patch electrodes were coated with surf wax (Mr Zogs Sex Wax; Zog Industries, Carpenteria, CA, USA). Patch electrodes were positioned on the IHC membrane using a PatchStar micromanipulator (Scientifica Ltd, Uckfield, UK). The patch pipette filling solution used for most of the whole-cell recordings was (mM): 106 caesium glutamate, 20 CsCl, 3 $MgCl_2$, 1 EGTA-CsOH, 5 Na_2ATP, 0.3 Na_2GTP, 5 Hepes-CsOH, 10 Na_2-phosphocreatine (pH 7.3, 294 mosmol kg^{-1}). For a few experiments different concentrations (0.1, 0.3, 1 and 5 mM) of the fast Ca^{2+} buffer BAPTA (Roche Diagnostic, UK) were used instead of 1 mM EGTA (Fluka, UK) in the above intracellular solution. In the BAPTA solutions the concentration of CsCl was adjusted to keep the osmolality constant. For the current clamp experiment, used to record the action potential applied to cells as a voltage protocol in Fig. 9, the pipette filling solution contained (mM): 131 KCl, 3 $MgCl_2$, 1 EGTA-KOH, 5 Na_2ATP, 5 Hepes-KOH, 10 sodium phosphocreatine (pH 7.3, 292 mosmol kg^{-1}). Data acquisition was performed using pCLAMP software with a Digidata 1320A/1440A interface (Molecular Devices). Depending on the protocols used, data were sampled at 5, 10, 20 or 100 kHz and filtered at 2.5, 5 or 10 kHz (8-pole Bessel) and stored on computer for off-line analysis (Origin; OriginLab Corp., Northampton, MA, USA; Mini Analysis Program:

Synaptosoft Inc., Decatur, GA, USA). Current recordings were corrected off-line for the linear leak conductance (g_{leak}) typically calculated between −84 mV and −74 mV (immature IHCs: 2.6 ± 0.1 nS, $n = 65$, P3–P9; adult IHCs 1.5 ± 0.1 nS, $n = 68$, P25–P69). Holding currents are plotted as zero current. Membrane potentials were corrected for the voltage drop across the uncompensated residual series resistance (R_s: 4.7 ± 0.1 MΩ, $n = 126$, compensation 0–80%) and for a liquid junction potential (LJP), measured between electrode and bath solutions, according to Neher (1992). The LJP was −11 mV for the caesium glutamate and −4 mV for the KCl intracellular solution. The average voltage-clamp time constant (product of R_s and membrane capacitance C_m) was 46 ± 1.0 μs ($n = 126$). For the experiments aimed at investigating the activation kinetics of I_{Ca} the average voltage-clamp time constant was 32 ± 3.0 μs ($n = 30$).

Extracellular superfusion

All voltage-clamp experiments were performed in the presence of 30 mM TEA and 15 mM 4-AP (Fluka, UK) in order to block the K^+ currents (immature: $I_{K,neo}$ and I_{K1}, Marcotti *et al.* 2003*a*; adult: $bE_{K,f}$ and $I_{K,s}$, Marcotti *et al.* 2004*a*). Moreover, the K^+ channel blockers apamin (300 nM: Calbiochem, UK) and linopirdine (80–100 μM: Tocris Bioscience, Bristol, UK) were also used to block I_{SK2} (in immature IHCs, Marcotti *et al.* 2004*b*) and $I_{K,n}$ (in adult IHCs, Marcotti *et al.* 2003*a*), respectively. When the concentration of added K^+-channel blockers was > 1 mM, or when 1.3 mM Ca^{2+} was replaced by either 5 mM Ca^{2+} or Ba^{2+}, NaCl was adjusted to keep the osmolality constant. Solutions containing drugs were applied through a multibarrelled pipette positioned close to the preparation.

Statistical analysis

Statistical comparisons of means were made by Student's two-tailed *t* test or, for multiple comparisons, analysis of variance, usually one-way ANOVA followed by Tukey's test. Two-way ANOVA, followed by the Bonferroni's test, was used to compare data sets from apical and basal regions of the cochlea. Mean values are quoted ± S.E.M. where $P < 0.05$ indicates statistical significance. In some of the figures statistical significance is indicated by asterisks.

Results

Calcium current in developing gerbil IHCs

The Ca^{2+} current (I_{Ca}) was isolated from the total membrane current by blocking all the K^+ currents present in IHCs using a cocktail of K^+ channel blockers (see Methods). A typical example of I_{Ca}, in the presence of 1.3 mM extracellular Ca^{2+}, recorded from apical-coil (Ac) and basal-coil (Bc) IHCs of the immature cochlea is shown in Fig. 1*A* and *B*, respectively. The average current–voltage (*I–V*) curves measured at the peak I_{Ca}, for both apical and basal immature gerbil IHCs, are shown in Fig. 1*C*. *I–V* curves for individual cells were fitted using the following equation:

$$I = \frac{g_{max}(V - V_{rev})}{1 + \exp\left(\frac{V_{½} - V}{S}\right)} \quad (1)$$

where I is the current, g_{max} is the maximum chord conductance, V is the membrane potential, V_{rev} is the reversal potential of the current, $VV_{½}$ is the potential at which the conductance is half-activated and S is the slope factor that defines the voltage sensitivity of current activation. The maximum size of I_{Ca} (measured at −15 mV) was found to be similar between apical (−408 ± 96 pA $n = 6$) and basal (−365 ± 37 pA $n = 5$) immature IHCs. I_{Ca} recorded from both apical and basal IHCs activated at around −70 mV (defined as 1% of g_{max}). No significant differences were observed in $V_{½}$ and S between the two cochlear regions.

The time constant of I_{Ca} activation at different membrane potentials was obtained by fitting the current recordings from apical (Fig. 1*D*) and basal (Fig. 1*E*) IHCs with the following equation:

$$I(t) = I_{max}\left(1 - \exp\left(\frac{-t}{\tau}\right)\right)^{\alpha} \quad (2)$$

where $I(t)$ is the current at time t, I_{max} is the peak I_{Ca}, τ is the time constant of activation and α was fixed as 2 (Zidanic & Fuchs, 1995; Marcotti *et al.* 2003*b*; Johnson *et al.* 2005), which is consistent with a Hodgkin–Huxley model with two opening gating particles (Hodgkin & Huxley, 1952). In some apical IHCs (about 50%), the onset of I_{Ca} at more hyperpolarized potentials appeared slow and possibly multicomponent (Fig. 1*A*), although this was not investigated further. Although the average size of I_{Ca} was similar between the two cell populations (Fig. 1*C*) the activation time constants (Fig. 1*F*) were significantly faster in basal than in apical IHCs ($P < 0.0001$ – two-way ANOVA; post test indicated significance at $P < 0.001$ between −61 mV and −46 mV).

The Ca^{2+} current recorded in adult apical (~300 Hz, P28) and basal (~30 kHz, P30) gerbil IHCs is shown in Fig. 2*A* and *B*, respectively. The maximum size of I_{Ca} measured at −11 mV in adult apical IHCs (Fig. 2*C*: −155 ± 22 pA, $n = 6$, P27-P30) was found to be slightly smaller than that of basal cells (−181 ± 21 pA, $n = 7$, P27–P30) but the difference was not quite significant ($P = 0.05$). The activation of I_{Ca} in both apical and basal adult IHCs occurred positive to −65 mV. Half-maximal activation and slope factor were not significantly different

between apical and basal IHCs (Fig. 2*C*). Surprisingly, $V_{1/2}$ activation was significantly more negative (about 10 mV) in immature than in adult IHCs ($P < 0.001$ for both cochlear regions: one-way ANOVA). Figure 2*D* shows the direct comparison of the peak I_{Ca} as a function of development and cochlear position. While the maximum size of I_{Ca} did not change significantly along the length of the cochlea within either age group, it was much smaller in adult compared to immature IHCs ($P < 0.001$), as previously observed in mouse IHCs (Marcotti *et al.* 2003*b*; Johnson *et al.* 2005, 2007). The activation time course of I_{Ca} in adult IHCs is shown on an expanded time scale in Fig. 2*E* and *F*. Similar to immature IHCs, the I_{Ca} activation time constants in adult basal IHCs were significantly faster than those of low-frequency cells (Fig. 2*G: P* < 0.0001 – two-way ANOVA; post test at $P < 0.001$ between −56 mV and −41 mV).

Although I_{Ca} is essential for numerous cellular processes (e.g. exocytosis and membrane excitability) it is very often investigated in mammals at room temperature instead of using body temperature. Therefore we performed a few experiments to determine whether the size of I_{Ca} was temperature dependent. A typical example of I_{Ca} recorded at room temperature from immature (P8) and adult (P51)

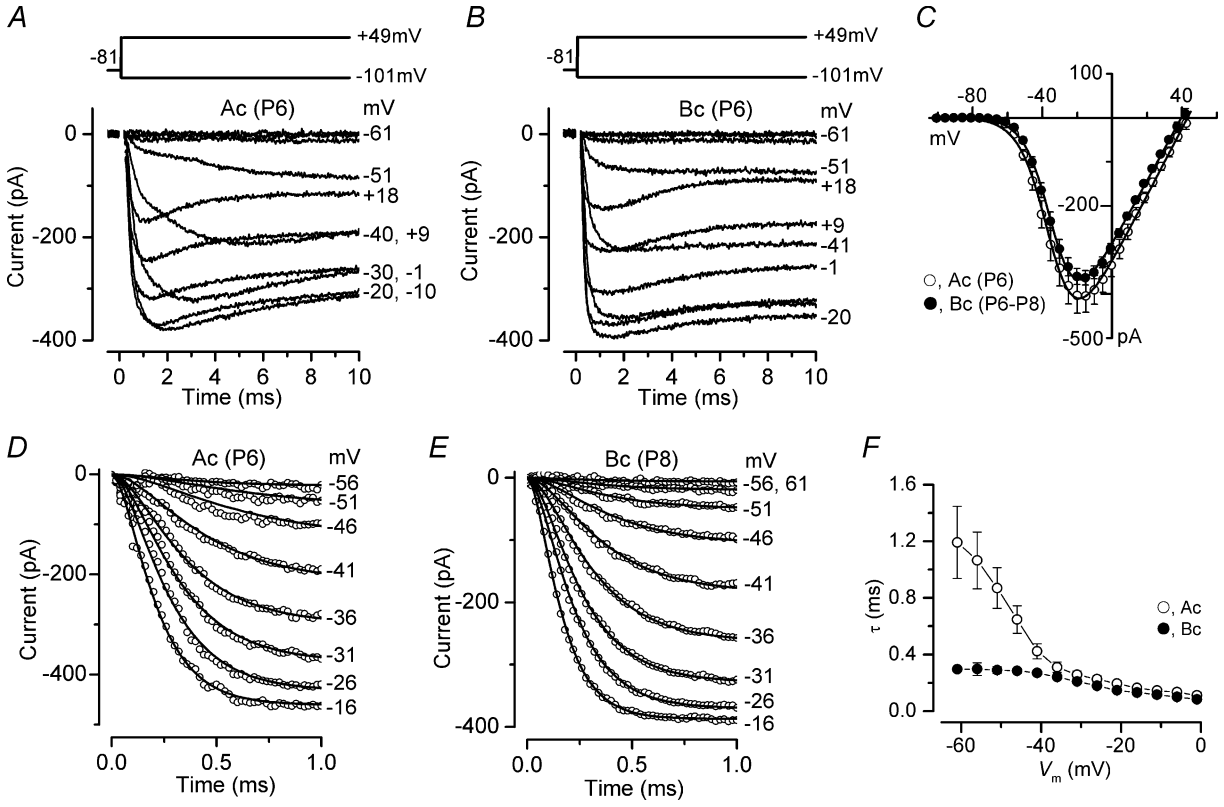

Figure 1. Ca^{2+} currents in immature gerbil IHCs
A and *B*, Ca^{2+} currents recorded from apical and basal IHCs, respectively. Currents were elicited by depolarizing voltage steps of 5 mV increments (10 ms in duration) from −101 mV starting from the holding potential of −81 mV. A schematic representation of the voltage protocol is shown above the current traces. For clarity only some of the traces are shown. In this and the following figures, actual test potentials, corrected for voltage drop across uncompensated R_s, are shown next to some of the traces. Residual capacitative transients have been blanked. Apical (*A*) and basal (*B*) I_{Ca} are averages from nine and seven protocol repetitions, respectively. Apical IHC: C_m 9.3 pF; R_s 5.3 MΩ; g_{leak} 2.4 nS. Basal IHC: C_m 8.1 pF; R_s 4.9 MΩ; g_{leak} 2.8 nS. *C*, Average peak current–voltage (*I–V*) curves for I_{Ca} obtained from 6 apical and 5 basal IHCs, including those shown in *A* and *B*. The continuous lines are fits using eqn (1) and the fitting parameters are: apical IHC $g_{max} = 7.6$ nS, $V_{rev} = 43.2$ mV, $V_{1/2} = -34.4$ mV, $S = 8.2$ mV; basal IHC $g_{max} = 7.3$ nS, $V_{rev} = 39.6$ mV, $V_{1/2} = -33.1$ mV, $S = 7.6$ mV. *D* and *E*, I_{Ca} recorded from apical and basal IHCs, respectively, on an expanded time scale (1 ms). Continuous lines are fits using eqn (2). The voltage protocol used was as in panels *A* and *B* and note that for clarity only a few current traces are shown and one in every two data points are plotted. Number of repetitions: three (Ac) and eight (Bc). Apical cell: C_m 7.7 pF; R_s 5.0 MΩ; g_{leak} 2.5 nS. Basal cell: C_m 7.4 pF; R_s 5.2 MΩ; g_{leak} 2.4 nS. *F*, time constants of activation for I_{Ca} recorded at different membrane potentials in apical (number of observations from left to right: 3, 5, 7, 7, 7, 7, 6, 5, 5, 6, 6, 6, 6) and basal (number of observations: 4, 8, 9, 9, 9, 9, 9, 9, 9, 8, 8, 7, 6) IHCs. Unless otherwise stated all recording in this and following figures are at near body temperature (34–37°C) and using 1.3 mM extracellular Ca^{2+}.

gerbil IHCs is shown in Fig. 3*A* and *B*, respectively. The maximum size of I_{Ca} in immature IHCs (-164 ± 19 pA, $n = 5$, Fig. 3*C*) was significantly smaller than that recorded at body temperature ($P < 0.0005$), giving a temperature sensitivity (Q_{10}) of 1.90 (ΔT used: 14°C). In adult IHCs, the maximum size of I_{Ca} measured at room temperature (-116 ± 13 pA, $n = 5$, Fig. 3*C*) was also significantly smaller compared to that recorded at body temperature ($P < 0.0001$). In adult IHCs the size of I_{Ca} changed with temperature with a Q_{10} of 1.36, indicating that somehow Ca^{2+} channels (most likely their open channel probability) become less temperature dependent with maturation. These results are similar to recent findings from mouse P14 IHCs ($Q_{10} = 1.1$ in whole cell: Nouvian, 2007).

Inactivation of the Ca^{2+} current in gerbil IHCs

In order to obtain a realistic representation of I_{Ca} inactivation it was important to completely block the small conductance Ca^{2+}-activated K^+ current SK2 (using 300 nM apamin: Marcotti *et al.* 2004*b*) since its presence in whole-cell recordings gives a false impression of a pronounced Ca^{2+} current inactivation (Schnee & Ricci, 2003; Marcotti *et al.* 2003*b*). Figure 4*A* shows some examples of inward Ca^{2+} currents recorded over a period of 600 ms in apical (middle panel) and basal (bottom panel) adult gerbil IHCs (P27–P30). Inactivation curves (Fig. 4*D*) were obtained by measuring the peak I_{Ca} during a 100 ms test step to -11 mV (apical IHC: Fig. 4*B*; basal IHC: Fig. 4*C*) following a series of 600 ms conditioning steps (Fig. 4*A*). The fits through the data were obtained using a modified first-order Boltzmann equation:

$$I = I_{const} + \frac{I_{max} - I_{const}}{1 + \exp\left(\frac{V - V_{1/2}}{S}\right)} \quad (3)$$

where I_{max} is the maximum size of I_{Ca}, I_{const} is the amplitude of the non-inactivating component of the Ca^{2+} current and the other parameters are as in eqn (1). For comparison, the inactivation curves obtained from apical

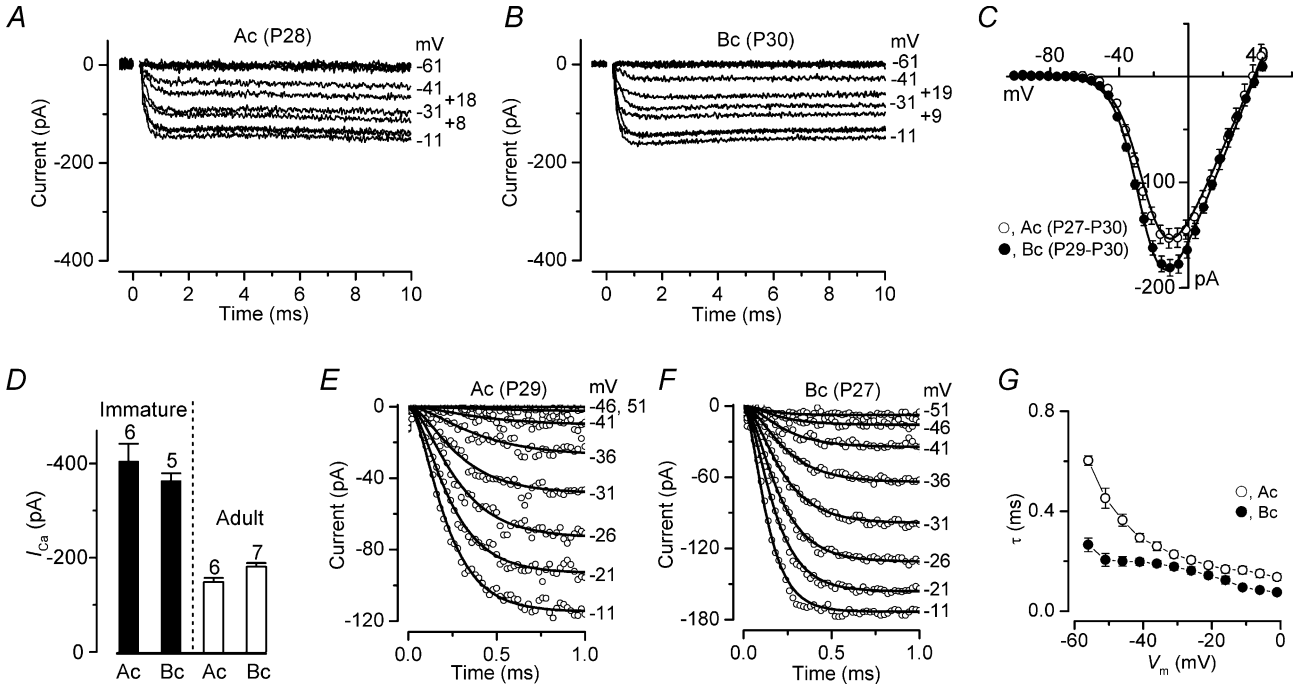

Figure 2. Ca^{2+} currents in adult gerbil IHCs
A and *B*, I_{Ca} recorded from apical (*A*) and basal (*B*) IHCs. Recordings were obtained using the same voltage protocol described in Fig. 1*A* and *B*. Note that for an easier comparison with immature data, the ordinate was kept as in Fig. 1*A* and *B*. I_{Ca} in apical (*A*) and basal (*B*) IHCs are averages from five and eight repetitions, respectively. Apical IHC: C_m 10.2 pF; R_s 6.1 MΩ; g_{leak} 2.6 nS. Basal IHC: C_m 11.7 pF; R_s 5.3 MΩ; g_{leak} 0.9 nS. *C*, Average peak *I–V* curves for I_{Ca} obtained from 6 apical and 7 basal IHCs, including those shown in *A* and *B*. The continuous lines are fits using eqn (1). Fitting parameters are: apical IHC $g_{max} = 3.8$ nS, $V_{rev} = 38.0$ mV, $V_{1/2} = -23.4$ mV, $S = 8.0$ mV; basal IHC $g_{max} = 4.1$ nS, $V_{rev} = 38.8$ mV, $V_{1/2} = -25.9$ mV, $S = 7.4$ mV. *D*, maximum size of I_{Ca} in apical and basal IHCs from immature (filled columns) and adult (open columns) gerbils. Number of cells investigated is shown above each column. *E* and *F*, I_{Ca} on an expanded time scale from apical (*E*) and basal (*F*) IHCs. Number of repetitions: five (Ac) and 10 (Bc). Continuous lines are fits using eqn (2). Apical cell: C_m 11.7 pF; R_s 3.9 MΩ; g_{leak} 2.9 nS. Basal cell: C_m 8.3 pF; R_s 4.9 MΩ; g_{leak} 1.0 nS. *G*, activation time constant of I_{Ca} at different membrane potentials in apical (number of observations: 2, 6, 9, 9, 9, 9, 9, 9, 8, 7, 6, 5) and basal (number of observations: 4, 5, 5, 5, 5, 5, 5, 5, 4, 3, 3, 3) IHCs.

and basal immature IHCs (P6–P8) are shown in Fig. 4*E*. The Ca^{2+} current is likely to be largely available at rest since the resting membrane potential of mammalian IHCs is usually between −55 mV and −70 mV in immature cells (Marcotti *et al.* 2003*a*) and −65 mV to −75 mV in adult cells (Marcotti *et al.* 2004*a*). This is assuming that the real resting potential of IHCs is similar to that recorded under patch clamp as opposed to the depolarized value obtained with more damaging *in vivo* intracellular recordings (−25 mV to −45 mV: Russell & Sellick, 1978). In adult IHCs the more hyperpolarized resting potential range *in vitro* could be a slight over-estimation since most of the depolarizing standing transducer current (gerbil IHCs: Jia *et al.* 2007) is likely to be missing. Figure 4*F* shows the fitting parameters for adult and immature IHCs derived from the curves in Fig. 4*D* and *E*. While $V_{½}$ (Fig. 4*F*, middle panel) and the slope factor (Fig. 4*F*, right panel) did not change significantly as a function of both development and cochlear region, the degree of I_{Ca} inactivation (Fig. 4*F*, left panel) was larger in basal ($58.0 \pm 4.5\%$ $n = 6$) compared to apical ($44.8 \pm 2.2\%$ $n = 6$, $P < 0.02$) adult IHCs.

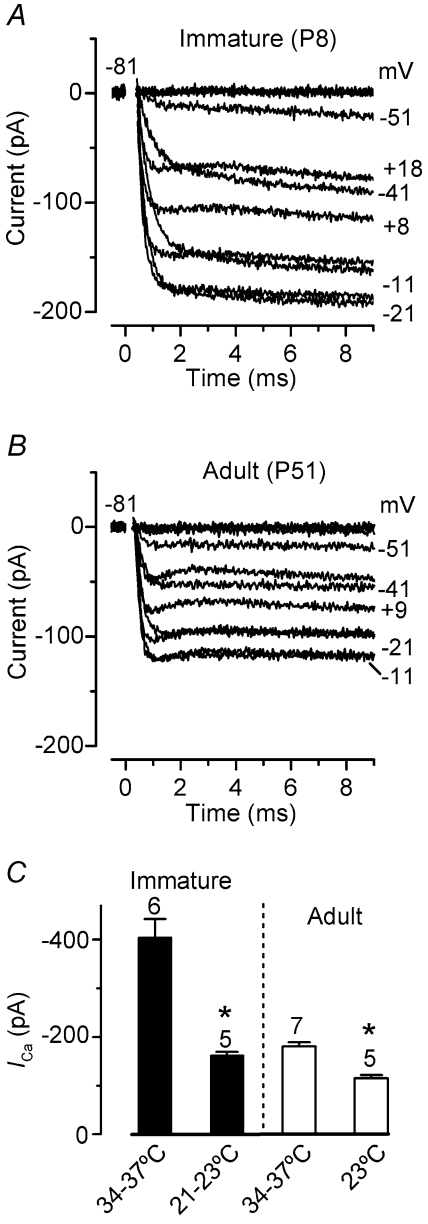

Figure 3. Ca^{2+} currents recorded at room temperature (21–23°C)
A and *B*, I_{Ca} recorded at room temperature from immature (Ac: 21°C) and adult (Bc: 23°C) IHCs, respectively. Recordings were obtained using the same voltage protocol described in Fig. 1. I_{Ca} in apical (*A*) and basal (*B*) IHCs are averages from 10 and 11 repetitions, respectively. Immature IHC: C_m 10.3 pF; R_s 6.0 MΩ; g_{leak} 2.4 nS. Adult IHC: C_m 9.6 pF; R_s 6.2 MΩ; g_{leak} 0.8 nS. *C*, comparison of the peak I_{Ca} in immature and adult IHCs at room and body temperature.

It is well established that Ca^{2+} channel inactivation can be driven by Ca^{2+}- and/or voltage-dependent processes (Budde *et al.* 2002). Therefore, we conducted a few experiments in which extracellular Ca^{2+} was increased from 1.3 mM to 5 mM to enhance the possible presence of Ca^{2+}-dependent channel inactivation. Furthermore, 5 mM Ca^{2+} was replaced with equimolar Ba^{2+}, a divalent cation that cannot induce Ca^{2+}-dependent inactivation. Figure 5*A* shows an example of inward currents elicited using a 600 ms depolarizing voltage step to −11 mV in the presence of 5 mM Ca^{2+} and 5 mM Ba^{2+}. The time course of both currents could be adequately fitted with a double exponential (see legend of Fig. 5 for details). Figure 5*B* shows the average *I–V* curves in the presence of 5 mM Ca^{2+} and 5 mM Ba^{2+} (P50, $n = 6$). The maximum current size in 5 mM Ba^{2+} (-241 ± 19 pA, $n = 6$ at −19 mV) was significantly larger than that in the presence in 5 mM Ca^{2+} (-200 ± 15 pA, $n = 6$, $P < 0.01$ paired *t* test). However, this difference could be underestimated since long-lasting voltage protocols (∼1 min) were used for these experiments and Ba^{2+} was mainly superfused onto IHCs after Ca^{2+}, possibly leading to a smaller Ba^{2+} current due to a partial current run-down. Inactivation curves (Fig. 5*E*) were obtained by measuring the peak current (5 mM Ca^{2+}: Fig. 5*C*, mM Ba^{2+}: Fig. 5*D*) obtained using the same voltage protocol described in Fig. 4*A–C*. The extent of inactivation in the presence of 5 mM Ba^{2+} (18%: Fig. 5*F*) was significantly reduced compared to both 5 mM Ca^{2+} (43%, $P < 0.01$) and 1.3 mM Ca^{2+} (50%; $P < 0.001$), suggesting the presence of both Ca^{2+}- and voltage-dependent inactivation processes. No significant difference was observed between 1.3 mM and 5 mM Ca^{2+} (Fig. 5*F*), although the inactivation–voltage relation in the latter had a more pronounced U-shaped appearance that resembled that of the *I–V* curve (Fig. 5*B*).

Calcium-dependent inactivation of the Ca^{2+} channels can be induced by global changes in the intracellular Ca^{2+} concentration such as by the release of Ca^{2+} from intracellular Ca^{2+} stores, known to be present in IHCs (Kennedy & Meech, 2002; Marcotti *et al.* 2004*a*), Ca^{2+}

entry through neighbouring Ca^{2+} channels or indeed Ca^{2+} accumulation following prolonged depolarization. In order to determine whether Ca^{2+} originating from these other (non-local) sources had any influence on the Ca^{2+}-dependent inactivation observed in IHCs, we used different concentrations of the fast Ca^{2+} buffer BAPTA instead of EGTA (Neher, 1998). Although both BAPTA and EGTA have similar affinities for Ca^{2+}, the former has a much higher binding rate constant allowing it to buffer increases in cytosolic Ca^{2+} closer to the source (Naraghi & Neher, 1997). Figure 6*A* shows some examples of I_{Ca} recorded from adult basal-coil IHCs in the presence of 1 mM EGTA (used for all recordings shown so far), 0.1 mM or 5 mM BAPTA in the intracellular solution. As shown in Fig. 6*B* the extent of I_{Ca} inactivation did not change significantly with the different buffering conditions (one-way ANOVA). To investigate further the possible effects of intracellular buffering on I_{Ca} inactivation, we fitted its time course using a double exponential, which adequately follows the inactivation process (see fits in Fig. 6*A*). The fast (Fig. 6*C*: τ_{fast}) but not the slow (Fig. 6*D*: τ_{slow}) time constant was slightly affected by substituting EGTA with BAPTA as intracellular Ca^{2+} buffer ($P < 0.02$, one-way ANOVA). These results suggest that the source of Ca^{2+} responsible for Ca^{2+} channel inactivation is likely to be very colocalized.

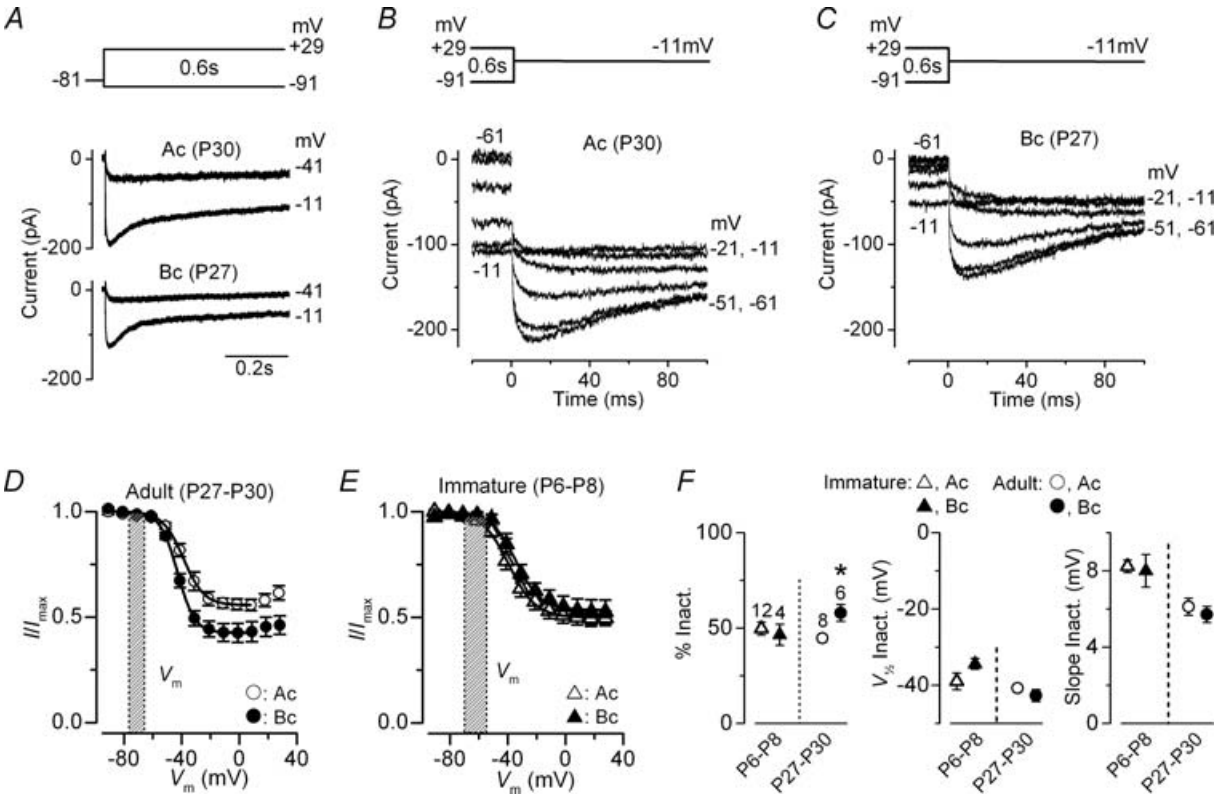

Figure 4. Ca^{2+} current inactivation

A, Ca^{2+} currents recorded from adult apical (middle panel) and basal (bottom panel) gerbil IHCs. Currents were elicited by depolarizing voltage steps (10 mV nominal increments and 600 ms in duration) from −91 mV starting from the holding potential of −81 mV. A schematic representation of the voltage protocol is shown above the current traces. For clarity only a few traces are shown and are not averages. Apical IHC: C_m 10.7 pF; R_s 4.1 MΩ; g_{leak} 2.5 nS. Basal IHC: C_m 8.3 pF; R_s 4.9 MΩ; g_{leak} 1.0 nS. *B* and *C*, Ca^{2+} tail currents recorded at a membrane potential of −11 mV after a series of depolarizing conditioning steps (600 ms) from −91 mV (see protocol in panel *A*). Residual capacitative transients have been blanked. Recordings in *B* and *C* are from the same apical and basal IHCs shown in *A*. *D* and *E*, average steady-state inactivation curves of I_{Ca} from adult (*D*: apical $n = 8$; basal $n = 6$) and immature (*E*: apical $n = 12$; basal $n = 4$) gerbil IHCs obtained using tail currents as described in *B* and *C*. The shaded areas delineate the resting membrane potential of IHCs recorded in patch clamp experiments. The continuous lines are fits up to the potential of maximum inactivation using eqn (3). Fitting parameters are: adult apical IHCs (*D*: ○) $I_{max} = -166$ pA, $I_{const} = 0.56$, $V_{1/2} = -38.8$ mV, $S = 7.2$ mV; adult basal IHCs (*D* ●) $I_{max} = -148$ pA, $I_{const} = 0.43$, $V_{1/2} = -42.9$ mV, $S = 6.0$ mV; immature apical IHCs (*E*: △) $I_{max} = -274$ pA, $I_{const} = 0.50$, $V_{1/2} = -39.3$ mV, $S = 9.3$ mV; immature basal IHCs (*E*: s) $I_{max} = -196$ pA, $I_{const} = 0.53$, $V_{1/2} = -34.4$ mV, $S = 8.7$ mV. *F*, average percentage (left panel), $V_{1/2}$ (middle panel) and slope (right panel) of inactivation obtained from fitting individual inactivation curves using eqn (3) (number of cells shown above the columns).

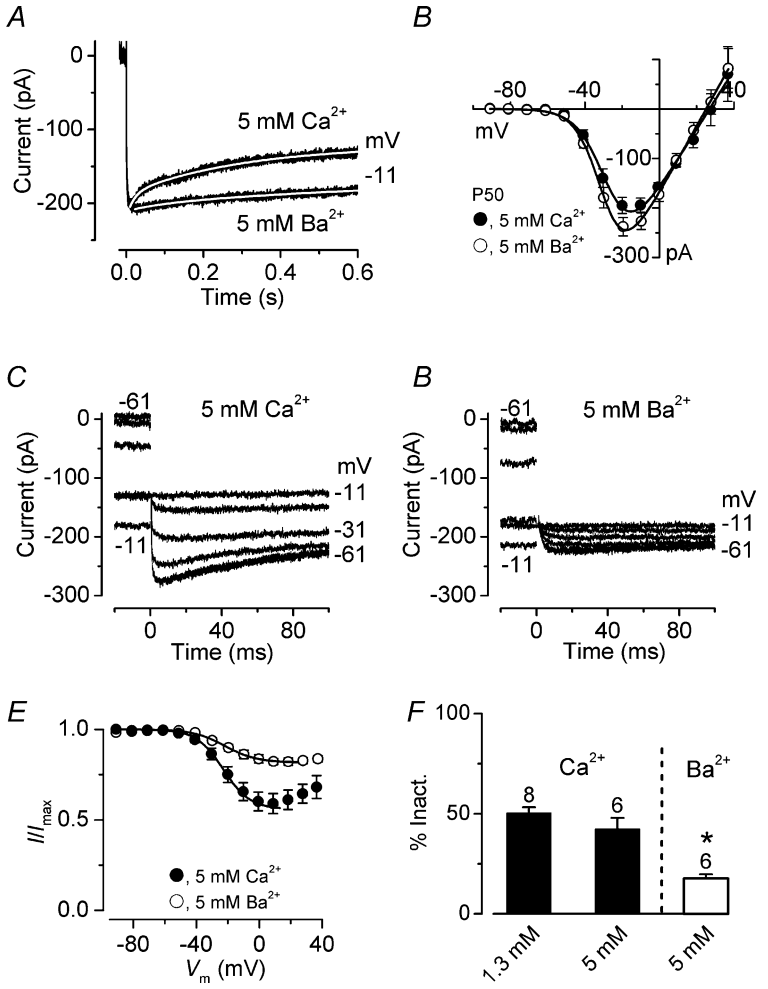

Figure 5. Ca^{2+} channel inactivation is reduced by barium
A, inward currents recorded during the superfusion of 5 mM Ca^{2+} or 5 mM Ba^{2+} from a P50 apical IHC in response to a 600 ms voltage step to −11 mV from a holding potential of −81 mV. Fits through the data were obtained using a double exponential equation. The fitting parameters are: 5 mM Ca^{2+} τ_{fast} 19 ms, τ_{slow} 299 ms; 5 mM Ba^{2+} τ_{fast} 86 ms, τ_{slow} 855 ms. Cell properties were: C_m 11.9 pF, R_s 6.3 MΩ, g_{leak} 1.7 nS. *B*, average *I–V* curves of peak inward currents in 5 mM Ca^{2+} or 5 mM Ba^{2+} from the same 6 IHCs (2 apical and 4 basal IHCs, P50). Continuous lines are fits using eqn (1). Fitting parameters are: 5 mM Ca^{2+} g_{max} 6.0 nS, V_{rev} 27 mV, $V_{1/2}$ −26.8 mV, S 7.6 mV; 5 mM Ba^{2+} g_{max} 6.8 nS, V_{rev} 25 mV, $V_{1/2}$ −29.2 mV, S 6.8 mV. *C* and *D*, inward tail currents recorded at a membrane potential of −11 mV after a series of depolarizing conditioning steps (600 ms) from −91 mV (see protocol in Fig. 4*A–C*). Residual capacitative transients have been blanked. Recordings in *C* and *D* are from the same IHC shown in *A*. *E*, average inactivation curves obtained by plotting the peak inward tail currents described in panels *C* and *D* (in 5 mM Ca^{2+} and 5 mM Ba^{2+}). The continuous lines are fits up to the potential of maximum inactivation using eqn (3). Fitting parameters are: 5 mM Ca^{2+} $I_{max} = -274$ pA, $I_{const} = 0.57$, $V_{1/2} = -23.3$ mV, $S = 9.3$ mV; 5 mM Ba^{2+} $I_{max} = -249$ pA, $I_{const} = 0.81$, $V_{1/2} = -21.7$ mV, $S = 10.1$ mV. *F*, average percentage of current inactivation obtained from fitting individual inactivation curves using eqn (3). For comparisons, the value obtained in 1.3 mM Ca^{2+} (from Fig. 4*F*) is also shown. Number of cells is shown above the columns.

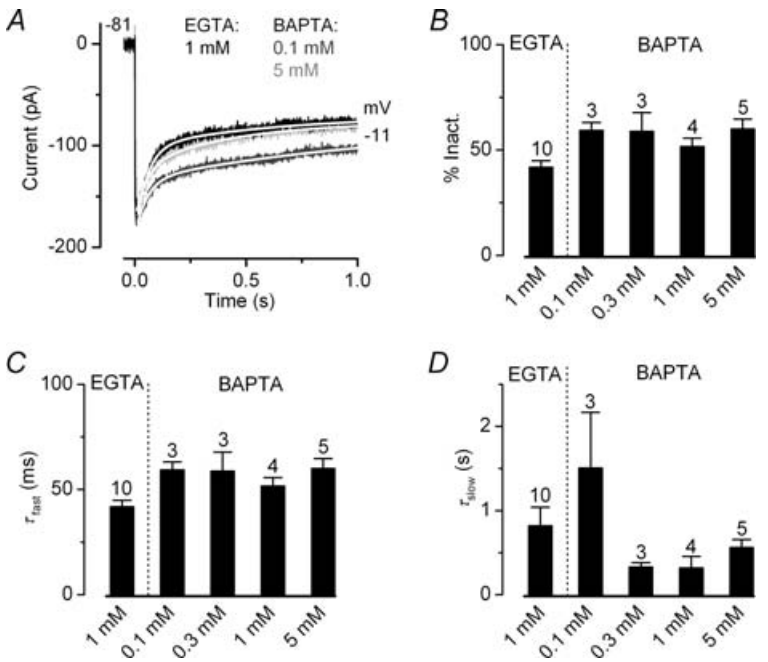

Figure 6. Ca^{2+} buffers do not prevent inactivation of the Ca^{2+} channels
A, Ca^{2+} currents recorded from adult basal IHCs in the presence of 1 mM EGTA (black), 0.1 mM BAPTA (dark grey) or 5 mM BAPTA (grey) in response to a 1 s voltage step to −11 mV from a holding potential of −81 mV. Fits through the data were obtained using a double exponential equation. The fitting parameters are: 1 mM EGTA τ_{fast} 52 ms, τ_{slow} 435 ms; 0.1 mM BAPTA τ_{fast} 54 ms, τ_{slow} 1181 ms, 5 mM BAPTA τ_{fast} 51 ms, τ_{slow} 589 ms. Cell properties were: 1 mM EGTA (P25) C_m 12.2 pF, R_s 4.7 MΩ, g_{leak} 0.8 nS; 0.1 mM BAPTA (P69) C_m 10.5 pF, R_s 5.4 MΩ, g_{leak} 0.9 nS; 5 mM BAPTA (P69) C_m 10.4 pF, R_s 4.2 MΩ, g_{leak} 0.6 nS. *B*, Average percentage of I_{Ca} inactivation using 1 mM EGTA (P25 basal IHCs) and different BAPTA (0.1, 0.3, 1 and 5 mM) concentrations (P69 basal IHCs). *C* and *D*, fast (τ_{fast}) and slow (τ_{slow}) time constants obtained by fitting the time course of I_{Ca} inactivation using a double exponential. Number of cells in *B–D* is shown above each column.

Functional implications of Ca^{2+} current inactivation

Neurotransmitter release at the IHC ribbon synapse is likely to be regulated by a few L-type Ca^{2+} channels (Brandt *et al.* 2005). The readily releasable pool (RRP), which represents the number of vesicles docked at the active zones (von Gersdorff *et al.* 1996; Moser & Beutner, 2000), is recruited when IHCs are stimulated using relatively short depolarizing voltage steps (up to around 100 ms at body temperature and using 1.3 mM extracellular Ca^{2+}: Johnson *et al.* 2005, 2007). Since the release of the RRP could be affected by I_{Ca} inactivation, we investigated how Ca^{2+} channels would respond to repeated stimulation. For this set of experiments, both immature and adult gerbil IHCs were depolarized using a series of voltage steps to −11 mV (50 ms in duration) every 150 ms (Fig. 7*A*). An example of I_{Ca} recordings, using the above protocol, from immature (P7) and adult (P25) IHCs is shown in Fig. 7*B*. In adult IHCs (Fig. 7*C*), repeated stimulation caused an initial decline in size of I_{Ca} (8% in apical and 11% in basal IHCs with the second stimulus) followed by a very similar shallow reduction, reaching a maximum inactivation (after 25 repetitions) of 20% in apical and 23% in basal cells. This result suggests that low- and high-frequency adult IHCs are likely to exhibit a similar recovery of I_{Ca} from inactivation. The slight variation in the degree of I_{Ca} inactivation between apical and basal IHCs (Fig. 7*C*) is likely to be due to their different steady-state inactivation (Fig. 4*D*). When the same voltage protocol was applied to immature IHCs the initial I_{Ca} inactivation increased from 12% and 7% (with the second stimulus) to 55% and 36% after 25 repetitions in apical and basal cells, respectively (Fig. 7*D*). The extent of this inactivation was significantly greater in apical than in basal IHCs ($P < 0.0001$: Fig. 7*D*), suggesting a more rapid recovery from I_{Ca} inactivation in the latter.

In order to investigate a possible difference in the rate of I_{Ca} recovery from inactivation in immature IHCs, apical and basal cells were subjected to a two-pulse protocol in which they were depolarized to −11 mV for 20 ms while changing the interpulse interval (IPI) from 10 ms up to 1.5 s (Fig. 8*A*). The relation between the normalized I_{Ca} and IPI, for both apical and basal immature IHCs (Fig. 8*B*), was adequately described using a single exponential function. As suggested by the results shown above (Fig. 7*D*), apical IHCs ($\tau = 106.0 \pm 8.7$ ms, $n = 5$) showed a significantly slower recovery from inactivation than basal cells ($\tau = 48.2 \pm 2.5$ ms, $n = 4$, $P < 0.001$).

Since apical and basal immature IHCs exhibited differences in the recovery of I_{Ca} from inactivation we sought to establish the physiological consequences of this on the cells' ability to maintain trains of Ca^{2+} action potentials (Marcotti *et al.* 2003*b*). To achieve this aim we recorded a spontaneous action potential (AP) from an immature gerbil IHC under current clamp conditions at 37°C and used it as a voltage protocol. To obtain a train of APs with frequencies of 4 Hz and 10 Hz the AP was repeatedly applied to the cell every 0.25 s and 0.1 s, respectively (Fig. 9*A*, left panel). Since the total duration of the recorded AP was about 80 ms, limiting the maximal frequency to 12.5 Hz, we tested a higher frequency by selecting 40 ms around the AP upstroke (Fig. 9*A*, right

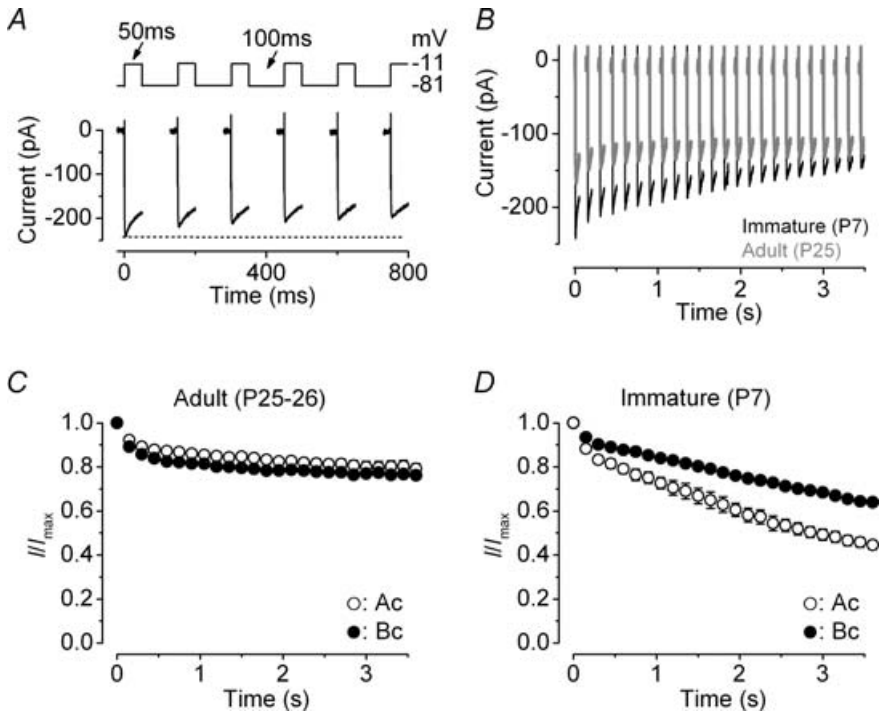

Figure 7. Ca^{2+} current inactivation during repetitive stimulation
A, Ca^{2+} currents recorded from an immature (P7) basal IHC in response to a train of 50 ms voltage steps to −11 mV from a holding potential of −81 mV. Time between voltage steps was 100 ms (see protocol: top panel). Note that for clarity only 800 ms (total protocol duration: 3.5 s) is shown. *B*, Ca^{2+} currents recorded from an immature (black) and an adult (grey) basal IHC. Immature IHC: C_m 7.7 pF, R_s 5.0 MΩ, g_{leak} 1.9 nS; Adult IHC: C_m 10.7 pF, R_s 4.8 MΩ, g_{leak} 0.8 nS. *C* and *D*, average peak Ca^{2+} current normalized to that elicited by the initial depolarizing step, obtained using the protocol described in *A* from adult (apical: $n = 6$; basal: $n = 4$) and immature (apical: $n = 3$; basal: $n = 5$) IHCs.

panel). The Ca^{2+} current recorded during the AP protocol at 4 Hz, 10 Hz and 25 Hz is shown in Fig. 9*B*, where for clarity only I_{Ca} responses to the first and the last AP are depicted. Figures 9*C* and *D* shows the size of the Ca^{2+} current, normalized to the initial current, induced by the APs as a function of time in apical and basal IHCs, respectively. When APs were repeated at 4 Hz the average size of I_{Ca} slightly increased with time in both apical and basal IHCs, reminiscent of prepulse facilitation of the Ca^{2+} channels (Dolphin, 1996). At 10 Hz, I_{Ca} in basal IHCs showed very little reduction (4%, Fig. 9*D*) compared to the more significant decrease in apical cells (12%, Fig. 9*C*, $P < 0.0001$), suggesting that the former could sustain APs at a higher frequency. A similar trend was also seen at 25 Hz (apical: 36%; basal: 30%, $P < 0.0001$). Although we did not measure the AP frequency in gerbil IHCs, our results indicate that the recovery of I_{Ca} from inactivation could allow basal cells to fire APs at a higher frequency than apical cells.

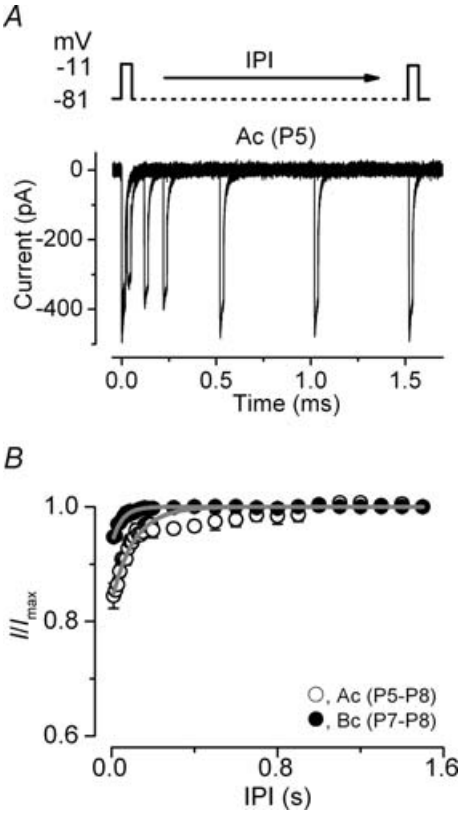

Figure 8. Recovery of the Ca^{2+} current from inactivation
A, Ca^{2+} currents elicited in an immature apical IHC in response to 20 ms depolarizing voltage steps to −11 mV (holding potential of −81 mV) at time 0 and varying the interpulse interval (IPI = from 10 ms to 1.5 s) after the initial step (schematic protocol shown above the current traces). Residual capacitative transients have been blanked. Cell properties were: C_m 8.5 pF, R_s 5.2 MΩ, g_{leak} 3.0 nS. *B*, peak Ca^{2+} currents normalized to that at time 0 against the IPI (Ac: $n = 5$; Bc: $n = 4$). The recovery of I_{Ca} from inactivation was fitted with a single exponential function.

Discussion

The aim of the present study was to investigate the biophysical properties of Ca^{2+} channels in developing gerbil inner hair cells (IHCs) positioned in the apical (low-frequency: ∼300 Hz) and basal (high-frequency: ∼30 kHz) regions of the cochlea using near physiological recording conditions (body temperature and 1.3 mM extracellular Ca^{2+}). Although most of this information is well established in lower vertebrate auditory organs (Zidanic & Fuchs, 1995; Schnee & Ricci, 2003), the existence of tonotopic differences in the biophysical properties of I_{Ca} in mammalian IHCs has never been investigated before. The information gained by this study will provide important insights into whether Ca^{2+} channels could be involved in the fine tuning of mammalian IHCs.

$Ca_V1.3$ Ca^{2+} channels in developing mammalian IHCs

IHCs are the primary sensory receptors of the mammalian cochlea responsible for signalling the perception of sound to the central nervous system via the vast majority (90–95%) of afferent auditory nerve fibres entering the cochlea (Ryugo, 1992). Before the onset of hearing, which in most rodents occurs at around P10–P12, immature IHCs fire spontaneous Ca^{2+}-dependent action potentials (Marcotti *et al.* 2003*a*, 2003*b*; Johnson *et al.* 2007), which are likely to be responsible for the normal morphological and physiological maturation of the cochlea (Johnson *et al.* 2007). Upon maturation, IHCs respond to incoming sound with rapid and graded receptor potentials (Palmer & Russell, 1986) that are transmitted onto auditory afferent fibres. IHC depolarization, induced by either spontaneous action potential activity or incoming sound, causes an influx of Ca^{2+} into cells via the opening of voltage-gated Ca^{2+} channels. Since Ca^{2+} channels are clustered and colocalized with IHC presynaptic active zones (Roberts *et al.* 1990; Tucker & Fettiplace, 1995) their activation triggers the release of neurotransmitter from ribbon synapses (Parsons *et al.* 1994; Moser & Beutner, 2000). In addition to this synaptic activity, Ca^{2+} channels are also responsible for regulating IHC membrane excitability (Marcotti *et al.* 2004*a*,*b*). More than 90% of the total Ca^{2+} current expressed in IHCs is carried by L-type α1D ($Ca_V1.3$) Ca^{2+} channels (Platzer *et al.* 2000; Koschak *et al.* 2001), suggesting that the properties of I_{Ca} could be similar in IHCs irrespective of position or age. $Ca_V1.3$ channels are also expressed in the electromotile outer hair cells (mouse: Knirsch *et al.* 2007) although their relative number and/or single channel conductance is likely to be smaller than in IHCs.

Here we show that in contrast to lower vertebrates (Schnee & Ricci, 2003) the size of I_{Ca} did not change significantly along the cochlea in both immature and adult

IHCs (Figs 1 and 2). However, as previously reported in mouse IHCs (Beutner & Moser, 2001; Marcotti *et al.* 2003*b*; Johnson *et al.* 2005), a substantial reduction of I_{Ca} occurred with development (Fig. 2*D*). Changing the recording conditions from body (35–37°C) to room (21–23°C) temperature caused a significant reduction in the size of I_{Ca} in both immature (< P12: $Q_{10} = 1.9$) and adult (> P20: $Q_{10} = 1.4$) gerbil IHCs. These results are similar to recent observations in 2-week-old mouse IHCs (Nouvian, 2007) where a reduction in the size of I_{Ca} at room temperature was observed ($Q_{10} = 1.1$, whole-cell recordings; $Q_{10} = 1.3$, perforated patch). The significantly greater temperature dependence of I_{Ca} in immature IHCs (Fig. 3*D*), suggests that some differences exist in the properties of Ca^{2+} channels between the two stages of development. The larger Ca^{2+} current at physiological temperature is likely to be caused by an increased open channel probability (Acerbo & Nobile, 1994).

At body temperature, the activation time course of I_{Ca} was significantly faster in IHCs located in the high-frequency region of the gerbil cochlea throughout development. This scenario is further complicated if we consider that I_{Ca} in adult IHCs (Fig. 2*E*–*G*) showed overall faster activation kinetics than that of immature cells (Fig. 1*D*–*F*). The activation time constant of I_{Ca} in gerbil basal IHCs (Figs 1*F* and 2*G*) was comparable to that recorded in mouse apical IHCs (physiological 1.3 mM extracellular Ca^{2+}: Marcotti *et al.* 2003*b*; Johnson *et al.* 2005; 2 mM Ca^{2+}: Nouvian, 2007) although no developmental difference was observed in the latter (Johnson *et al.* 2005). Although we did not investigate the activation kinetics of I_{Ca} at room temperature, previous studies on mouse IHCs have clearly reported that lowering the temperature from ~37°C to room temperature slowed its activation time constant by about half (Marcotti *et al.* 2003*b*; Nouvian, 2007). A further difference between I_{Ca} in immature and adult IHCs was the 10 mV depolarizing shift in the voltage range of I_{Ca} activation ($V_{½}$: immature IHCs: −33 mV; adult: −23 mV). The reason for this developmental shift, assuming that it occurs *in vivo*, is currently unknown, although the activation of I_{Ca} in IHCs at both stages is likely to be within the range of the cell resting membrane potential (Fig. 4*D* and *E*). A similar shift with IHC maturation has recently been reported in rat IHCs (Knirsch *et al.* 2007).

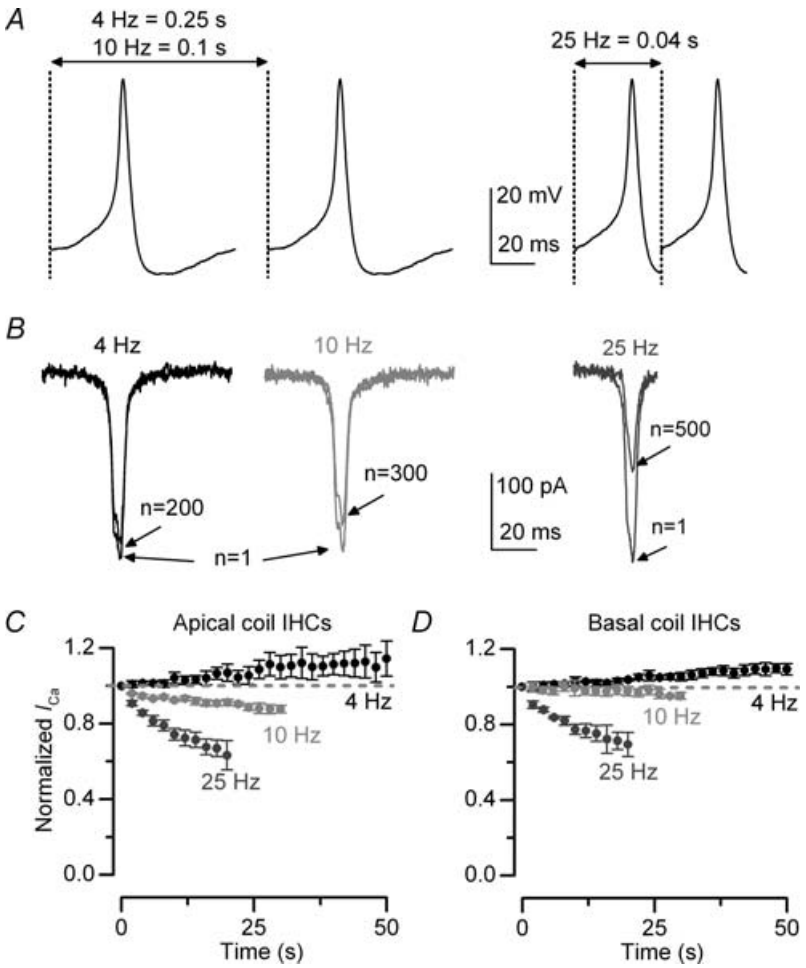

Figure 9. Ca^{2+} current inactivation and action potential activity
A, spontaneous action potential (AP) recorded from an immature gerbil IHC under current clamp conditions at 37°C and using 1.3 mM extracellular Ca^{2+}. Cell properties were: C_m 9.7 pF, R_s 3.2 MΩ, V_m −60 mV. Left panel: APs were applied to immature IHCs as a voltage command, from the holding potential of −61 mV, and repeated every 0.25 ms and 0.1 ms to obtain the desired frequencies of 4 Hz and 10 Hz, respectively. The total duration of the AP was 80 ms. Right panel: in order to achieve a frequency of 25 Hz, only part (40 ms) of the AP shown in the left panel was used as a best compromise. *B*, example of Ca^{2+} currents recorded from an apical IHC in response to the first and last AP in a train applied at the different frequencies as shown in *A*. Cell properties were: C_m 10 pF, R_s 8.9 MΩ, g_{leak} 4.1 nS. *C* and *D*, peak I_{Ca} in response to APs normalized to the initial current (in response to the first AP) as a function of time in both apical (*C*: 4 Hz $n = 5$; 10 Hz $n = 3$; 25 Hz $n = 4$) and basal (*D*: 4 Hz $n = 3$; 10 Hz $n = 3$; 25 Hz $n = 2$) IHCs. For clarity, only one data point every 2 s is shown. Note that the degree of inactivation increased with AP frequency and was more pronounced in apical IHCs.

Inactivation of $Ca_V1.3$ Ca^{2+} channels in gerbil IHCs

Recent investigations have shown that I_{Ca} in auditory hair cells inactivates, although the degree of inactivation appears to vary depending on the cell investigated (Marcotti *et al.* 2003*b*; Schnee & Ricci, 2003; Lee *et al.* 2007). Ca^{2+} channel inactivation provides a negative feedback mechanism to adjust the available Ca^{2+} current and is used to regulate a variety of physiological processes in both neuronal and non-neuronal cells (von Gersdorff & Matthews, 1996). Inactivation of the Ca^{2+} channel can be induced by either Ca^{2+} or voltage (Budde *et al.* 2002). Our results show that the extent of Ca^{2+} channel inactivation was largely reduced by Ba^{2+} (Fig. 5), indicating that Ca^{2+}-dependent inactivation (CDI) is predominant in gerbil IHCs. This was also supported by the fact that the relation between I_{Ca} inactivation and voltage (Fig. 5*E*) in the presence of high Ca^{2+} roughly resembles that of its U-shaped *I–V* curve (Fig. 5*B*; Brehm & Eckert, 1978). Similar results have previously been described in lower vertebrates (Schnee & Ricci, 2003; Lee *et al.* 2007). Furthermore, I_{Ca} also showed voltage-dependent inactivation (VDI), since the inactivation of the Ba^{2+} current (Fig. 5*E*) through the Ca^{2+} channels increased with voltage and tended to saturate at positive potentials. A comparable degree of Ca^{2+} current inactivation was observed between immature (apical: 50%; basal: 47%) and adult (apical: 45%; basal: 58%) IHCs, even though the size of I_{Ca} in the latter was about a third. However, high-frequency adult IHCs showed a significantly larger Ca^{2+} channel inactivation than low-frequency cells (Fig. 4*E*), suggesting possible differences in the channel itself or in the control of local Ca^{2+} homeostasis between the two cochlear locations. This steady-state inactivation of I_{Ca} is likely to have a greater effect on the physiological voltage responses of adult IHCs (especially on the DC receptor potentials of basal cells) than those of immature cells (low-frequency action potentials). Possible roles for CDI in adult IHCs could be to regulate the number of available Ca^{2+} channels at the ribbon synapses and/or prevent Ca^{2+} loading. Less likely is its role in afferent fibre adaptation since this occurs on a faster time scale and is most likely caused by a reduced release of synaptic vesicle over time (Goutman & Glowatzki, 2007).

CDI can be brought about by the increase of cytosolic Ca^{2+} near the Ca^{2+} channel caused by current through the channel itself, adjacent Ca^{2+} channels, Ca^{2+} release from intracellular stores or the accumulation of Ca^{2+} following long-lasting cell depolarization. In order to determine how close the Ca^{2+} source was to the Ca^{2+} channel, and therefore attempt to discriminate between the above possibilities, we used different concentrations of intracellular BAPTA (Fig. 6) instead of EGTA. Our results show that 5 mM BAPTA did not significantly affect the CDI, suggesting that in gerbil IHCs the Ca^{2+} source for CDI is likely to be within 18 nm of each Ca^{2+} channel (Naraghi & Neher, 1997; Neher, 1998). These findings differ from those described in lower vertebrates where 1 mM BAPTA was sufficient to affect CDI in chick auditory hair cells (Lee *et al.* 2007), indicating a more distant coupling (about 40 nm) between Ca^{2+} channels and the Ca^{2+} source. Although we have not tested the possible direct modulation of CDI by Ca^{2+} stores (Lee *et al.* 2007) it is likely that the influx of Ca^{2+} from the opening of a single voltage-gated Ca^{2+} channel could cause CDI in gerbil IHCs (as seen in ventricular myocytes: Imredy & Yue, 1992) via the interaction of the Ca^{2+}-sensing protein calmodulin with the channel α-subunit (Peterson *et al.* 1999). This could explain the comparable degree of inactivation observed between immature and adult IHCs.

Repetitive maximal stimulation of I_{Ca} revealed another important difference between immature and adult IHCs, with a less extensive reduction in the size of I_{Ca} in adult cells over time (Fig. 7). This suggests that I_{Ca} in both apical and basal adult IHCs is able to sustain the repeated release of vesicles from the readily releasable pool (von Gersdorff *et al.* 1996; Moser & Beutner, 2000), which is essential for sound encoding. Although I_{Ca} inactivation is in theory less vital in immature IHCs (see above) we found position-dependent differences in its recovery from inactivation (Fig. 8*C*). The functional implication of this was that the maximum action potential frequency supported in apical IHCs is likely to be lower than that in basal cells (Fig. 9), suggesting that a difference in the spontaneous firing rate could exist along the mammalian cochlea. A similar action potential frequency in apical IHCs has been previously reported in the mouse ($\sim$4 Hz: Marcotti *et al.* 2003*b*; Johnson *et al.* 2007). It is possible that this intrinsic limit in the firing activity prevents large influx of Ca^{2+} into developing IHCs, which could alter their normal functional development (Johnson *et al.* 2007). Alternatively, it could be responsible for creating a tonotopic signal that guides the organization of the auditory system before the onset of sensory-driven activity (Stellwagen & Shatz, 2002).

Our results indicate that although $>90\%$ of I_{Ca} in mammalian IHCs is carried by $Ca_V1.3$ Ca^{2+} channels their activation and inactivation properties change with development and cochlear position pointing towards some differences in their structure or modulation. Splice variants of the $\alpha1$ subunit (Kollmar *et al.* 1997) together with differences in the accessory subunits (Catterall, 2000) could be responsible for the diverse biophysical properties observed in this study. Moreover, Ca^{2+}-dependent inactivation of I_{Ca} in IHCs could be modulated by a subtype of calmodulin-like Ca^{2+}-binding protein (CaBP: Yang *et al.* 2006). Additional CaBPs such as calbindin D_{28k}, calretinin and parvalbumin, generally assumed to play a role in intracellular Ca^{2+} buffering and known to be expressed in IHCs (Hackney *et al.* 2005),

also function as Ca^{2+} sensors (Berggard *et al.* 2002). Evidence also points towards a role for calbindin D_{28k} in modulating CDI of L-type Ca^{2+} channels (Lee *et al.* 2006). It would be informative to assess whether there is a differential expression of these proteins between low- and high-frequency adult gerbil IHCs.

In this study we have shown that the biophysical properties of I_{Ca} changed as a function of development. We suggest that these differences are likely to fulfil the different functional requirements of prehearing (spontaneous action potential activity) and mature (rapid and graded receptor potentials) IHCs. In addition, we also provide the first evidence for the existence of tonotopic differences in I_{Ca} throughout development, indicating that $Ca_V1.3$ Ca^{2+} channels are likely to be finely tuned by the expression of splice variants of the $\alpha 1$ subunit, different auxiliary subunits and/or specific Ca^{2+} binding proteins.

References

Acerbo P & Nobile M (1994). Temperature dependence of multiple high voltage activated Ca^{2+} channels in chick sensory neurones. *Eur Biophys J* **23**, 189–195.

Art JJ & Fettiplace R (1987). Variation of membrane properties in hair cells isolated from the turtle cochlea. *J Physiol* **385**, 207–242.

Berggard T, Miron S, Onnerfjord P, Thulin E, Akerfeldt KS, Enghild JJ, Akke M & Linse S (2002). Calbindin D28k exhibits properties characteristic of a Ca^{2+} sensor. *J Biol Chem* **277**, 16662–16672.

Beutner D & Moser T (2001). The presynaptic function of mouse cochlear inner hair cells during development of hearing. *J Neurosci* **21**, 4593–4599.

Brandt A, Khimich D & Moser T (2005). Few $Ca_V1.3$ channels regulate the exocytosis of a synaptic vesicle at the hair cell ribbon synapse. *J Neurosci* **25**, 11577–11585.

Brehm P & Eckert R (1978). Calcium entry leads to inactivation of calcium channel in *Paramecium*. *Science* **202**, 1203–1206.

Budde T, Meuth S & Pape HC (2002). Calcium-dependent inactivation of neuronal calcium channels. *Nat Rev Neurosci* **3**, 873–883.

Catterall WA (2000). Structure and regulation of voltage-gated Ca^{2+} channels. *Annu Rev Cell Dev Biol* **16**, 521–555.

Dallos P (1992). The active cochlea. *J Neurosci* **12**, 4575–4585.

Dolphin AC (1996). Facilitation of Ca^{2+} current in excitable cells. *Trends Neurosci* **19**, 35–43.

Fuchs PA, Evans MG & Murrow BW (1990). Calcium currents in hair cells isolated from the cochlea of the chick. *J Physiol* **429**, 553–568.

Fuchs PA, Nagai T & Evans MG (1988). Electrical tuning in hair cells isolated from the chick cochlea. *J Neurosci* **8**, 2460–2467.

Glowatzki E & Fuchs PA (2002). Transmitter release at the hair cell ribbon synapse. *Nat Neurosci* **5**, 147–154.

Goutman JD & Glowatzki E (2007). Time course and calcium dependence of transmitter release at the single ribbon synapse. *Proc Natl Acad Sci U S A* **104**, 16341–16346.

Greenwood DD (1990). A cochlear frequency-position function for several species – 29 years later. *J Acoust Soc Am* **87**, 2592–2605.

Hackney CM, Mahendrasingam S, Penn A & Fettiplace R (2005). The concentration of calcium buffereing proteins in mammalian cochlear hair cells. *J Neurosci* **25**, 7867–7886.

Hodgkin AL & Huxley AF (1952). A quantitative description of membrane current and its application to conduction and excitation in nerve. *J Physiol* **117**, 500–544.

Imredy JP & Yue DT (1992). Submicroscopic Ca^{2+} diffusion mediates inhibitory coupling between individual Ca^{2+} channels. *Neuron* **9**, 197–207.

Jia S, Dallos P & He DZ (2007). Mechanoelectric transduction of adult inner hair cells. *J Neurosci* **27**, 1006–1014.

Johnson SL, Adelman JP & Marcotti W (2007). Genetic deletion of SK2 channels in mouse inner hair cells prevents the developmental linearization in the Ca^{2+} dependence of exocytosis. *J Physiol* **583**, 631–646.

Johnson SL, Marcotti W & Kros CJ (2005). Spontaneous action potential activity in immature inner hair cells varies with cochlear position. *J Physiol* **563**, 177–191.

Kennedy HJ & Meech RW (2002). Fast Ca^{2+} signals at mouse inner hair cell synapse: a role for Ca^{2+}-induced Ca^{2+} release. *J Physiol* **539**, 15–23.

Knirsch M, Brandt N, Braig C, Kuhn S, Hirt B, Munkner S, Knipper M & Engel J (2007). Persistence of $Ca_v1.3$ Ca^{2+} channels in mature outer hair cells supports outer hair cell afferent signaling. *J Neurosci* **27**, 6442–6451.

Kollmar R, Fak J, Montgomery LG & Hudspeth AJ (1997). Hair cell-specific splicing of mRNA for the $\alpha 1D$ subunit of voltage-gated Ca^{2+} channels in the chicken's cochlea. *Proc Natl Acad Sci U S A* **94**, 14889–14893.

Koschak A, Reimer D, Huber I, Grabner M, Glossmann H, Engel J & Striessnig J (2001). $\alpha 1D$ (Cav1.3) subunits can form L-type Ca^{2+} channels activating at negative voltages. *J Biol Chem* **276**, 22100–22106.

Lee S, Briklin O, Hiel H & Fuchs PA (2007). Calcium-dependent inactivation of calcium channels in cochlear hair cells of the chicken. *J Physiol* **583**, 909–922.

Lee D, Obukhov AG, Shen Q, Liu Y, Dhawan P, Nowycky MC & Christakos S (2006). Calbindin-D28k decreases L-type calcium channel activity and modulates intracellular calcium homeostasis in response to K^+ depolarization in a rat β cell line RINr1046–38. *Cell Calcium* **39**, 475–485.

Marcotti W, Johnson SL, Holley MC & Kros CJ (2003*a*). Developmental changes in the expression of potassium currents of embryonic, neonatal and mature mouse inner hair cells. *J Physiol* **548**, 383–400.

Marcotti W, Johnson SL & Kros CJ (2004*a*). Effects of intracellular stores and extracellular Ca^{2+} on Ca^{2+}-activated K^+ currents in mature mouse inner hair cells. *J Physiol* **557**, 613–633.

Marcotti W, Johnson SL & Kros CJ (2004*b*). A transiently expressed SK current sustains and modulates action potential activity in immature mouse inner hair cells. *J Physiol* **560**, 691–708.

Marcotti W, Johnson SL, Rüsch A & Kros CJ (2003*b*). Sodium and calcium currents shape action potentials in immature mouse inner hair cells. *J Physiol* **552**, 743–761.

Martini M, Rossi ML, Rubbini G & Rispoli G (2000). Calcium currents in hair cells isolated from semicircular canals of the frog. *Biophys J* **78**, 1240–1254.

Mikaelian D & Ruben RJ (1965). Development of the hearing in the normal CBA-J mouse. *Acta Otolaryngol* **59**, 451–461.

Moody WJ & Bosma MM (2005). Ion channel development, spontaneous activity, and activity-dependent development in nerve and muscle cells. *Physiol Rev* **85**, 883–941.

Moser T & Beutner D (2000). Kinetics of exocytosis and endocytosis at the cochlear inner hair cell afferent synapse of the mouse. *Proc Natl Acad Sci U S A* **97**, 883–888.

Müller M (1996). The cochlear place-frequency map of the adult and developing Mongolian gerbil. *Hear Res* **94**, 148–156.

Naraghi M & Neher E (1997). Linearized buffered Ca^{2+} diffusion in microdomains and its implications for calculation of $[Ca^{2+}]$ at the mouth of a calcium channel. *J Neurosci* **17**, 6961–6973.

Neher E (1992). Correction for liquid junction potentials in patch clamp experiments. *Methods Enzymol* **207**, 123–131.

Neher E (1998). Vesicle pools and Ca^{2+} microdomains: new tools for understanding their roles in neurotransmitter release. *Neuron* **20**, 389–399.

Nouvian R (2007). Temperature enhances exocytosis efficiency at the mouse inner hair cell ribbon synapse. *J Physiol* **584**, 535–542.

Palmer AR & Russell IJ (1986). Phase-locking in the cochlear nerve of the guinea-pig and its relation to the receptor potential of inner hair-cells. *Hear Res* **24**, 1–15.

Parsons TD, Lenzi D, Almers W & Roberts WM (1994). Calcium-triggered exocytosis and endocytosis in an isolated presynaptic cell: capacitance measurements in saccular hair cells. *Neuron* **13**, 875–883.

Peterson BZ, DeMaria CD, Adelman JP & Yue DT (1999). Calmodulin is the Ca^{2+} sensor for Ca^{2+}-dependent inactivation of L-type calcium channels. *Neuron* **22**, 549–558.

Platzer J, Engel J, Schrott-Fischer A, Stephan K, Bova S, Chen H, Zheng H & Striessnig J (2000). Congenital deafness and sinoatrial node dysfunction in mice lacking class D L-type Ca^{2+} channels. *Cell* **102**, 89–97.

Ricci AJ, Gray-Keller M & Fettiplace R (2000). Tonotopic variations of calcium signalling in turtle auditory hair cells. *J Physiol* **524**, 423–436.

Roberts WM, Jacobs RA & Hudspeth AJ (1990). Colocalization of ion channels involved in frequency selectivity and synaptic transmission at presynaptic active zones of hair cells. *J Neurosci* **10**, 3664–3684.

Rodriguez-Contreras A & Yamoah EN (2001). Direct measurement of single-channel Ca^{2+} currents in bullfrog hair cells reveals two distinct channel subtypes. *J Physiol* **534**, 669–689.

Russell IJ & Sellick PM (1978). Intracellular studies of hair cells in the mammalian cochlea. *J Physiol* **284**, 261–290.

Ryugo DK (1992). The auditory nerve: peripheral innervation, cell body morphology, and central projections. In *The Mammalian Auditory Pathway: Neuroanatomy*, ed.Webster DB, Popper AN & Fay RR, pp. 23–65. Springer, New York.

Schnee ME & Ricci AJ (2003). Biophysical and pharmacological characterization of voltage-gated calcium currents in turtle auditory hair cells. *J Physiol* **549**, 697–717.

Spassova M, Eisen MD, Saunders JC & Parsons TD (2001). Chick cochlear hair cell exocytosis mediated by dihydropyridine-sensitive calcium channels. *J Physiol* **535**, 689–696.

Stellwagen D & Shatz CJ (2002). An instructive role for retinal waves in the development of retinogeniculate connectivity. *Neuron* **33**, 357–367.

Tucker T & Fettiplace R (1995). Confocal imaging of calcium microdomains and calcium extrusion in turtle hair cells. *Neuron* **15**, 1323–1335.

von Gersdorff H & Matthews G (1996). Calcium-dependent inactivation of calcium current in synaptic terminals of retinal bipolar neurons. *J Neurosci* **16**, 115–122.

von Gersdorff H, Vardi E, Matthews G & Sterling P (1996). Evidence that vesicles on the synaptic ribbon of retinal bipolar neurons can be rapidly released. *Neuron* **16**, 1221–1227.

Woolf NK & Ryan AF (1984). The development of auditory function in the cochlea of the Mongolian gerbil. *Hear Res* **13**, 277–283.

Wu YC, Art JJ, Goodman MB & Fettiplace R (1995). A kinetic description of the calcium-activated potassium channel and its application to electrical tuning of hair cells. *Prog Biophys Mol Biol* **63**, 131–158.

Yang PS, Alseikhan BA, Hiel H, Grant L, Mori MX, Yang W, Fuchs PA & Yue DT (2006). Switching of Ca^{2+}-dependent inactivation of $Ca_v1.3$ channels by calcium binding proteins of auditory hair cells. *J Neurosci* **26**, 10677–10689.

Zhang LI & Poo M (2001). Electrical activity and development of neural circuits. *Nat Neurosci* **4**, 1207–1214.

Zidanic M & Fuchs PA (1995). Kinetic analysis of barium currents in chick cochlear hair cells. *Biophys J* **68**, 1323–1336.

Acknowledgements

This work was supported by the Wellcome Trust and Deafness Research UK. WM is a Royal Society University Research Fellow. We would like to thank M. Cardwell and L. Williams for their excellent assistance with the gerbils.